

Rossby Wave Phase Speed Influences Heatwave Location through a Shift in Storm Track Position

Wolfgang Wicker¹, Nili Harnik², Maria Pyrina³, Daniela I. V. Domeisen^{1,3}

¹Faculty of Geosciences and Environment, University of Lausanne, Lausanne, Switzerland

²Porter School of the Environment and Earth Sciences, Tel Aviv University, Tel Aviv, Israel

³Department of Environmental Systems Science, ETH Zurich, Zurich, Switzerland

Key Points:

- Synoptic-scale wave phase speed is a function of the latitudinal storm track position.
- Phase speed determines where heatwaves occur by shaping temporal-mean circulation anomalies.
- Mean anticyclonic flow in the upper-troposphere is more important for the number of heatwave days than the mean heatwave duration.

14 **Abstract**

15 Surface anticyclones connected to the ridge of an upper-tropospheric Rossby wave are
 16 the dynamical drivers of mid-latitude summer heatwaves. It is, however, unclear to which
 17 extent an anomalously low zonal phase speed of the wave in the upper troposphere is
 18 necessary for persistent temperature extremes at the surface. Here, we use spectral anal-
 19 ysis to estimate a categorical phase speed for synoptic-scale waves. A composite anal-
 20 ysis of ERA5 reanalysis data reveals how a meridional shift in the Rossby wave packet
 21 envelope associated with a change in phase speed alters the geographically phase-locked
 22 stationary wave pattern. In both composites for amplified low or high phase speed waves,
 23 respectively, the ridges and troughs of these temporal-mean wave trains show enhanced
 24 and reduced heatwave frequency. The phase speed of synoptic-scale waves is, hence, cru-
 25 cial for where, but less important for whether heatwaves occur.

26 **Plain Language Summary**

27 High pressure systems tend to be associated with mid-latitude summer heatwaves,
 28 defined as multiple consecutive hot days. The persistence criterion in the heatwave def-
 29 inition raises the question whether the associated high pressure system has to be anom-
 30 lously persistent as well. Using a combination of observational data and atmospheric model
 31 output that is commonly regarded as ground truth for prediction purposes we find that
 32 this is not the case. By re-distributing the location of on-average high air pressure, some
 33 regions experience an increased heatwave frequency even if the atmospheric circulation
 34 is less persistent than usual. Understanding the link between persistent surface temper-
 35 ature extremes and the atmospheric circulation is important for the prediction and pro-
 36 jection of extreme events in a warming climate.

37 **1 Introduction**

38 The increased frequency in hot temperature extremes is a direct consequence of an-
 39 thropogenic climate change (Meehl & Tebaldi, 2004; Coumou et al., 2013; Fischer & Knutti,
 40 2015; S. Russo et al., 2015; E. Russo & Domeisen, 2023). Surface heat extremes that last
 41 several days, commonly referred to as heatwaves, adversely impact morbidity and can
 42 cause excess mortality (e.g., Ebi et al., 2021). Adaptation to and prediction of such ex-
 43 treme events, hence, requires a better understanding of heatwave drivers (Domeisen et
 44 al., 2023). The increase in heatwave frequency due to climate change is at least partly

45 driven by thermodynamic feedbacks with the land surface involving latent and sensible
46 heat fluxes (Fischer et al., 2007; Miralles et al., 2014; Hauser et al., 2016). On the other
47 hand, it remains unclear whether or to what extent atmospheric dynamics contribute
48 to the more frequent temperature extremes under climate change. Anticyclonic circu-
49 lation anomalies in the upper troposphere provide a necessary ingredient for mid-latitude
50 summer heatwaves (Schneidereit et al., 2012; Pfahl & Wernli, 2012; Sousa et al., 2018)
51 and, in particular, synoptic-scale waves with zonal wavenumbers in the range of 6-8 have
52 been identified as dynamical heatwave drivers (Kornhuber et al., 2019; Di Capua et al.,
53 2021). A focus is often set on slow-moving anticyclones or stationary waves (Jiménez-
54 Esteve & Domeisen, 2022; Jiménez-Esteve et al., 2022).

55 In mid-latitudes, synoptic-scale disturbances are usually associated with the fastest-
56 growing mode of moist baroclinic instability and marked as transient waves by an east-
57 ward phase propagation. Petoukhov et al. (2013), on the other hand, proposed a mech-
58 anism termed *quasi-resonant amplification* to explain the occurrence of amplified sta-
59 tionary synoptic-scale waves, using a monochromatic wave ansatz that expresses a cir-
60 cumglobal wave train with zero frequency. By deducing characteristics of the wave from
61 properties of the zonal-mean state, this mechanism projects an increase in persistent weather
62 extremes in a warmer climate, based solely on dry dynamics without thermodynamic feed-
63 backs, with a strong and narrow jet creating an efficient waveguide (Mann et al., 2017).
64 However, the applicability of the underlying theory such as *WKBJ* ray tracing techniques
65 has been questioned, calling for an improved definition of waveguidability (Wirth, 2020;
66 Wirth & Polster, 2021; White et al., 2022).

67 Instead of monochromatic normal modes that are used to develop the quasi-resonant
68 amplification mechanism, metrics of regional jet waviness (Röthlisberger et al., 2016) or
69 the amplitude of localized Rossby wave packets (Fragkoulidis et al., 2018) constitute an
70 alternative representation of the anticyclone that generates a heatwave. A range of typ-
71 ical mid-latitude processes governs the evolution of Rossby wave packets, i.e., cycloge-
72 nesis, downstream development, and wave breaking (e.g., Wirth et al., 2018). The en-
73 ergy propagation of localized wave packets can be expressed by a spatial group veloc-
74 ity vector field. The case in which the energy propagation is faster than the phase prop-
75 agation is termed *downstream development* and can be readily understood for barotropic
76 waves via the Rossby wave dispersion relation (Rossby, 1945; Yeh, 1949). For baroclinic
77 waves, on the other hand, vortex stretching can produce new circulation extremes both

78 downstream and upstream of the original disturbance (Simmons & Hoskins, 1979). Re-
 79 current Rossby wave packets where troughs and ridges repeatedly amplify in the same
 80 location can be particularly impactful for weather extremes such as heatwaves, cold spells,
 81 floods, and droughts (Zschenderlein et al., 2018; Röhlisberger et al., 2019; Ali et al., 2021).

82 It seems fair to assume that the persistence of near-surface temperatures inherent
 83 to the heatwave definition requires a similarly persistent atmospheric circulation, although
 84 it is not clear whether this notion of atmospheric persistence should apply only region-
 85 ally, or for the state of the entire hemisphere as suggested by the stationary circumglobal
 86 wave train perspective (Petoukhov et al., 2013; Mann et al., 2017; Kornhuber et al., 2019;
 87 Di Capua et al., 2021). Rossby wave phase speed is a manifest measure of atmospheric
 88 persistence and has indeed been connected with mid-latitude temperature extremes (Riboldi
 89 et al., 2020). However, the phase speed metric by Riboldi et al. (2020) is a weighted es-
 90 timate for zonal wavenumbers 1-15 and the reported linkage between phase speed and
 91 heatwaves has to be interpreted bearing in mind the clear relationship between phase
 92 speed and wavenumber from linear theory. We develop a categorical phase speed esti-
 93 mate of "*amplified slow*" versus "*amplified fast*" defining the range of low and high phase
 94 speeds for each wavenumber individually and focusing on zonal wavenumbers 5-8 (see
 95 Sec. 2.1). Based on this categorical estimate, we then present a composite analysis of
 96 upper-tropospheric low-frequency variability, Rossby wave packet diagnostics, and heat-
 97 wave frequency for episodes of low and high phase speed, respectively.

98 2 Data and Methods

99 In this study, we conduct a statistical analysis of ERA5 reanalysis data (Hersbach
 100 et al., 2020) for boreal summer (June-August, JJA) for the period 1959-2021. The back-
 101 ward extension of the ERA5 set grants a larger sample size but renders a temperature
 102 detrending necessary for heatwave diagnosis to account for anthropogenic climate change
 103 (see Sec. 2.2). For convenience, the pressure level data is downsampled to the horizon-
 104 tal resolution of a $2^\circ \times 2^\circ$ regular grid and 6-hourly temporal resolution which is suffi-
 105 cient for an accurate estimation of synoptic-scale wave phase speed (see Sec. 2.1). For
 106 the heatwave diagnosis, we use daily maximum 2m temperature computed from 1-hourly
 107 resolution data on a $0.5^\circ \times 0.5^\circ$ regular grid.

108 **2.1 Categorical Phase Speed Estimate**

109 In order to diagnose upper-tropospheric Rossby wave phase speed, we compute Hayashi
 110 spectra (Hayashi, 1979) of meridional wind anomalies at every grid point on the 250hPa
 111 surface between 35°N-65°N following the methodology of Randel and Held (1991). This
 112 involves a two-dimensional Fourier transformation of gridded meridional wind anom-
 113 alies defined with respect to the local climatology at each grid point. Power spectral den-
 114 sity is then averaged meridionally in coordinates of zonal wavenumber and phase speed
 115 (see the supporting information for technical details). Prior to the spectral analysis, the
 116 time series of meridional wind is divided into 30-day windows with a Hanning window
 117 taper and 50% overlap to obtain a time series of phase speed spectra. The largest de-
 118 tectable phase speed associated with the Nyquist frequency and the phase speed reso-
 119 lution of the spectral analysis depend both on zonal wavenumber and latitude. For the
 120 6-hourly time resolution and 30-day window length, we obtain a maximum phase speed
 121 of 85 ms^{-1} and a phase speed resolution of 1.4 ms^{-1} for wavenumber 7 at 50°N, for ex-
 122 ample. The non-zero temporal mean anomaly of individual 30-day windows used as in-
 123 put for the spectral analysis is identified as a zero-phase speed wave.

124 Since the goal of this study is to analyze the role of phase speed on temperature
 125 extremes, the continuous phase speed spectrum is divided into a "slow" and a "fast" phase
 126 speed bin for each wavenumber individually at the respective centroid of the JJA climatological-
 127 mean Hayashi spectrum (Fig. 1). Composites of power spectral density, meridional wind,
 128 heatwave frequency and Rossby wave packets are constructed by selecting 30-day episodes
 129 based on a 90th percentile threshold criterion for integrated meridional wind variance
 130 in the respective phase speed bin. Specifically, the meridional wind variance is summed
 131 for zonal wavenumbers $k = 5, \dots, 8$ to focus on synoptic-scale variability. This way, ei-
 132 ther composite, "amplified slow" or "amplified fast", is composed of 31 windows distributed
 133 over 23 and 25 years, respectively, without a clustering at one end of the time series in-
 134 dicative of a trend. There is, however, a dependence on the seasonal cycle with more "am-
 135 plified slow" occurrences in early than in late summer, and fewer "amplified fast" esti-
 136 mates in central summer than at the margins. The significance of composite means and
 137 composite variances is estimated using a parametric bootstrap similar to a Student's t-
 138 test and F-test, respectively.

139 **2.2 Rossby Wave Packet and Heatwave Diagnostics**

140 In addition to 30-day mean upper-tropospheric wind anomalies, Rossby wave packet
 141 and heatwave diagnostics provide means for analysing intra-composite variability at a
 142 higher temporal resolution, 6-hourly and daily, respectively. The envelope and phase of
 143 a Rossby wave packet can be calculated as the absolute value and argument of the complex-
 144 valued Hilbert transform of 6-hourly meridional wind anomalies (Zimin et al., 2003). The
 145 local phase speed is estimated using finite differences in time and longitude provided that
 146 the envelope surpasses a threshold of 15 ms^{-1} (Fragkoulidis & Wirth, 2020).

147 The heatwave detection algorithm is based on daily maximum temperatures at 2
 148 m height that are detrended by regressing the local time series on the time series of 9-
 149 year lowpass filtered global-mean surface air temperature to account for the strong ther-
 150 modynamic trend in the reanalysis data. Heatwave days are then defined as the exceedances
 151 of the 90th percentile of the local empirical probability distribution of detrended surface
 152 air temperatures lasting for at least three consecutive days (e.g., S. Russo et al., 2015).

153 **3 Results from Composite Analysis**

154 The JJA climatological-mean Hayashi spectrum for upper-tropospheric meridional
 155 wind in the Northern hemisphere mid-latitudes shows maximum power spectral density
 156 for zonal wavenumbers 5 to 8 (Fig. 1a). From baroclinic Rossby wave dynamics and re-
 157 cent studies of upper-tropospheric Hayashi spectra (e.g., Jiménez-Esteve et al., 2022),
 158 we expect an increasing phase speed with increasing zonal wavenumber. This expecta-
 159 tion is confirmed by Figure 1. While long waves (wavenumbers 2-4) show a phase speed
 160 distribution nearly symmetric around zero and can be considered stationary, shorter wave-
 161 lengths (wavenumber 6-9) are predominantly eastward propagating, as indicated by the
 162 centroid of the phase speed distribution (solid black line in Fig. 1).

163 Properties of the categorical phase speed estimate "amplified slow" versus "am-
 164 plified fast" as defined in Section 2.1 are illustrated as composite-mean power spectral
 165 density anomalies (Fig. 1b, c). For both categories, spectral power is enhanced in the
 166 respective phase speed bin without significantly altering spectral power in the opposing
 167 phase speed bin. In other words, the "amplified slow" composite-mean anomaly is roughly
 168 centered around a phase speed of 0 ms^{-1} , whereas the "amplified fast" composite in-
 169 dicates pronounced eastward phase propagation on the order of 5 ms^{-1} . The indepen-

170 dence of composites seen in power spectral density anomalies is a result of tuning the
171 spectral analysis, i.e., the choice of a 30-day window as explained in the supplementary
172 material, and ensures that the signal of high-phase speed waves is not simply caused by
173 the absence of low-phase speed waves. On the other hand, composite-mean anomalies
174 of power spectral density are largest in proximity to the centroid of the climatological-
175 mean phase speed distribution. Hence, there is no clear indication of a bimodal phase
176 speed behaviour which could provide a natural choice for separating the two phase speed
177 bins. Choosing the centroid of the climatological mean spectrum ensures approximately
178 equal variance in either phase speed bin, both in the climatological mean and the composite-
179 mean anomaly.

180 Particularly impactful summer heatwaves are found to be associated with multi-
181 week or monthly-mean circulation anomalies in the mid- or upper troposphere (e.g., García-
182 Herrera et al., 2010; Schneidereit et al., 2012; Kornhuber et al., 2019; Yiou et al., 2020),
183 commonly interpreted as the signature of stationary waves. To systematically assess the
184 importance of phase speed for creating temporal-mean wave structures, we conduct a
185 composite analysis of 30-day mean meridional wind anomalies at 250hPa based on our
186 categorical phase speed estimate (Fig. 2). Given the composite-mean power spectral den-
187 sity anomalies in Figure 1, we expect enhanced low-frequency variability or stationary
188 wave power in the "amplified slow" composite. This expectation is confirmed by the com-
189 posite variance of 30-day mean anomalies with a statistically significantly enhanced vari-
190 ance compared to climatology from the mid-latitude Pacific across North America to the
191 Atlantic (Fig. 2a). The low-frequency variability in the "amplified fast" composite, on
192 the other hand, is not significantly different from climatology (Fig. 2b).

193 A less expected picture is drawn by the composite-mean anomalies, which show sig-
194 nificant values of similar magnitude for both composites, throughout the mid-latitudes
195 but especially over the Eurasian continent (Fig. 2c, d). Interestingly, the "amplified slow"
196 composite highlights a mode with higher meridional wavenumber than the "amplified
197 fast" case. The crucial difference between the composite-mean signal and the compos-
198 itive variance is that the weak stationary wave in the composite mean has a significant lon-
199 gitudinal phase preference and can be described as geographically phase-locked. With-
200 out such phase preference, any stationary wave contributes to the composite variance,
201 not the composite mean. We note in particular that finding a significant composite-mean
202 signal for episodes with amplified high phase speed waves does not agree with a normal

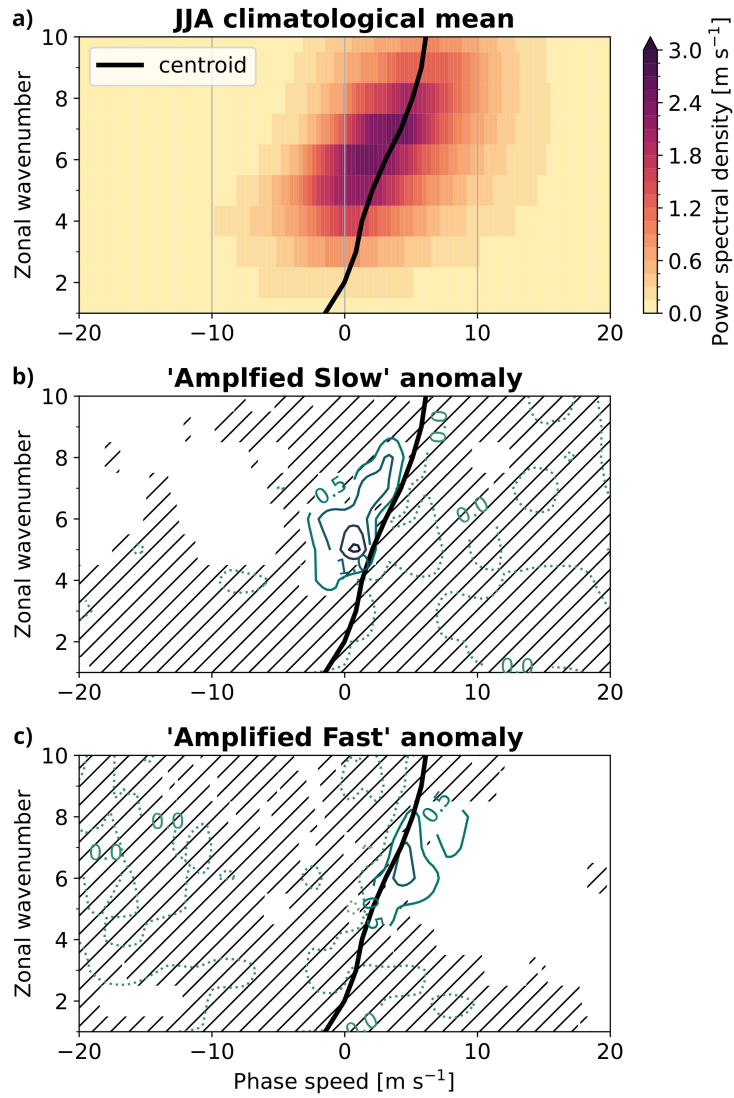


Figure 1. Meridional-mean (35°N - 65°N) power spectral density of meridional wind at 250hPa.

The solid black line indicates the centroid of the climatological mean spectrum separating the 'slow' and 'fast' phase speed bins. Hatching in panel b and c indicates where episodes with meridional wind variance exceeding the 90th percentile in the respective phase speed bin do not produce a statistically significant composite-mean anomaly at the 95% confidence level.

mode wave ansatz of constant wave amplitude in longitude and time where the eastward phase propagation would efface any composite mean different from zero. The mean signal can, however, be explained by localized Rossby wave packets, downstream development, or recurrent cyclogenesis (e.g., Wirth et al., 2018; Röhlisberger et al., 2019). As long as the wave energy in one location is intermittent and the timing of significant energy is synchronised with the phase of the wave, rapid phase propagation does not efface the temporal-mean signal.

As explained in Section 2.1, the composite analysis in Figure 2 is based on a criterion for meridional wind variance aggregated over the range of wavenumbers 5-8. The results are qualitatively similar when focusing on individual wavenumbers (see Fig. S2). More specifically, the mean anomaly for the composites based on the wavenumber range is close to the sum of composite-mean anomalies for individual wavenumbers. Also note that, since the upper-tropospheric wind is, to first order, horizontally non-divergent, an anomalous meridional wind also requires composite-mean zonal wind anomalies (Fig. S3a, b). In addition to the strong wavy component of the zonal wind anomalies, the zonal-mean zonal wind shows a southward shift for the "amplified slow" composite and a widening of the climatological jet for the "amplified fast" composite (Fig. S3c).

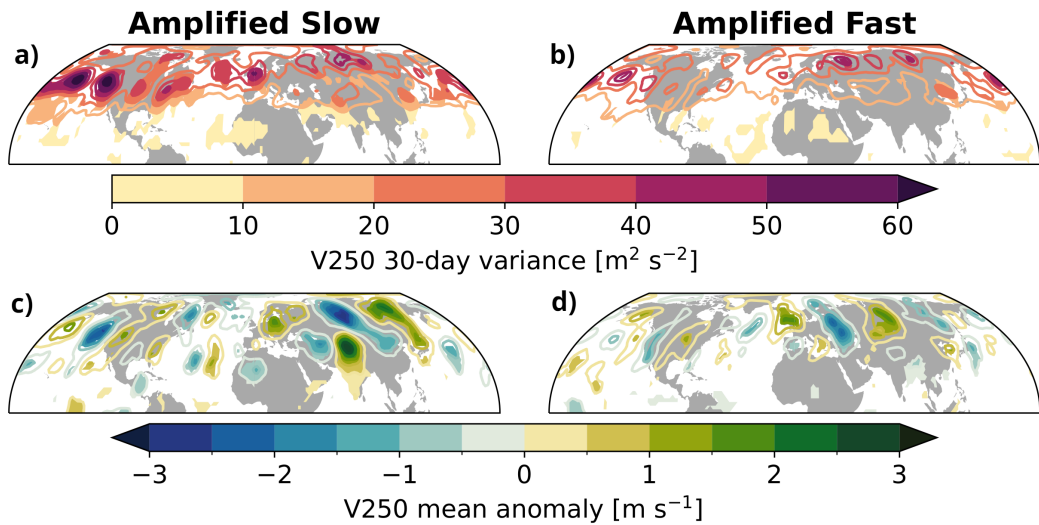


Figure 2. Variance (a, b) and mean (c, d) of 30-day mean upper-tropospheric meridional wind anomalies during for the composites as defined for Figure 1; color shading indicates a statistically significant increase in variance or a composite mean significantly different from zero at the 95% confidence level.

Motivated by the finding of a significant composite-mean signal for amplified waves with rapid phase propagation, we seek for further insight by analysing meridional wind variability at 6-hourly resolution in terms of Rossby wave packet diagnostics. In the climatological boreal summer mean (Fig. 3a, b), the Rossby wave packet envelope highlights the mid-latitude storm track of baroclinic waves maximizing over the North Pacific and North Atlantic ocean basins. Similarly, the climatological-mean phase speed maximizes in the location of the strong westerly jets. In addition, there is a clear latitudinal dependence with reduced or easterly phase speed on the equatorward side of our mid-latitude domain. These estimates agree well with the climatology computed by Frakouolidis and Wirth (2020).

Assessing the composite-mean phase speed anomalies (Fig. 3d, f), the significant and zonally symmetric reduction in phase speed north of 35°N for the "amplified slow" composite compared to climatology validates our categorical phase speed estimate with a local phase speed metric. But we also note an intriguing increase in phase speed compared to climatology in the subtropics, possibly an indication of mid-latitude baroclinic waves penetrating further south. The "amplified fast" composite, on the other hand, exhibits a more uniform increase in phase speed across the Northern hemisphere. Given the composite criterion with a percentile threshold on meridional wind variance it is not surprising to see mostly positive composite-mean Rossby wave envelope anomalies (Fig. 3c, e). It is, however, visible that positive anomalies for the "amplified slow" composite are concentrated south of the climatological maximum, whereas for the "amplified fast" composite, the Rossby wave envelope is enhanced in place with the climatological maximum with a noticeable reduction over the Mediterranean region. The difference in composite-mean envelope anomalies indicates an equatorward displacement of upper-tropospheric waves during episodes of low zonal phase speed.

The initial hypothesis of this study was that a reduced upper-tropospheric phase speed would increase the frequency of persistent temperature extremes at the surface. Therefore, Figure 4 shows the composite-mean summer heatwave frequency anomalies in units of heatwave days per 30-day time window (climatological mean value ≈ 1.5 days/window in the Northern hemisphere). Statistically significant anomalies found across the Northern Hemisphere for both composites exhibit a zonally asymmetric structure with both increased and reduced heatwave frequencies. The similarity of the two maps of composite-mean anomalies, instead of a dominant increase in heatwave frequency for the "ampli-

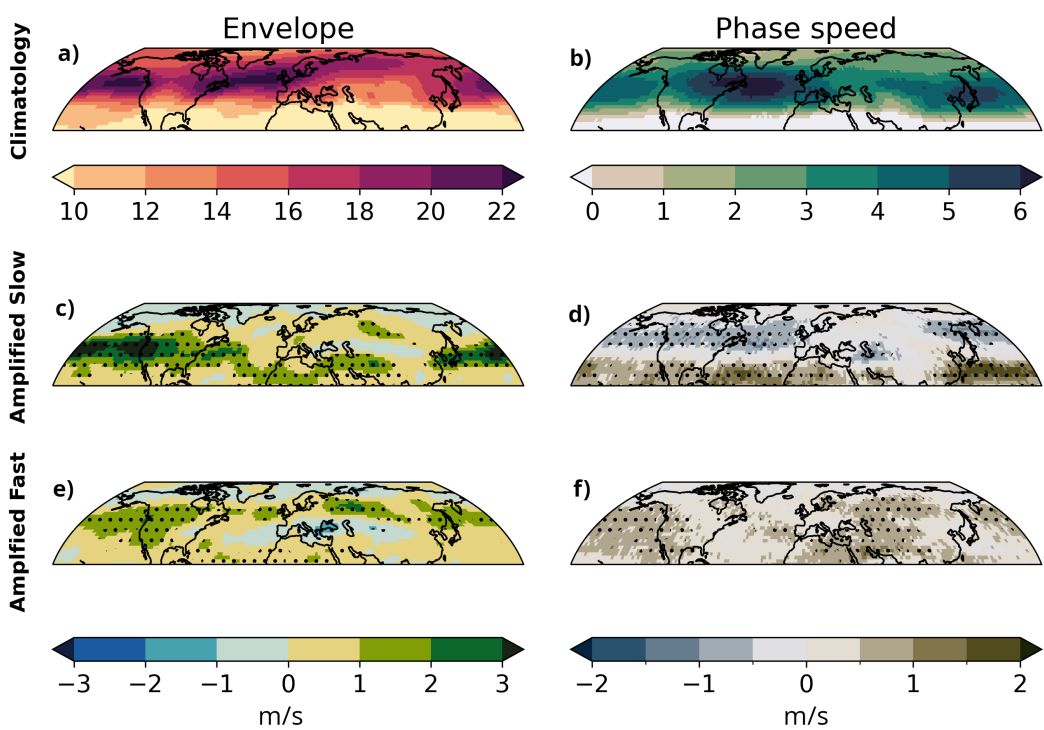


Figure 3. Climatological-mean Rossby wave packet envelope and phase speed (panel a, b) and mean anomalies (panel c, d, e, f) for composites as defined for Figure 1. Stippling indicates statistical significance at a 95% confidence level.

253 fied slow" composite suggested by the enhanced power of stationary waves, falsifies the
254 initial hypothesis stated above. However, that similarity does not disprove the influence
255 of the upper-tropospheric circulation on surface heatwave frequency.

256 Comparing the geographically phase-locked composite-mean wave trains (bottom
257 row Fig. 2) with Figure 4, we find that regions of enhanced composite-mean heatwave
258 frequency co-locate with composite-mean anticyclonic circulation anomalies. For the "am-
259 plified slow" composite, regions of enhanced heatwave frequency and anticyclonic circu-
260 lation comprise, for example, the Southern United States and Western Russia, whereas
261 Mongolia and Western Canada are highlighted in the "amplified fast" composite. The
262 upper-tropospheric influence on surface temperature extremes in these regions is further
263 emphasized by positive and negative anomalies in the climatological-mean heatwave du-
264 ration (Fig. 4c). Specifically, the climatological-mean heatwave duration is limited to less
265 than four days in areas where heatwave occur preferentially during episodes of rapid phase
266 propagation, while the mean heatwave duration can exceed five days in areas that ex-
267 perience mean anticyclonic anomalies during episodes of slow phase propagation. This
268 sensitivity is, however, not strong enough to produce a significant signal in the heatwave
269 frequency.

270 To understand why the power of stationary waves illustrated by the composite vari-
271 ance of 30-day mean anomalies (Fig. 2a, b) does not exert the expected influence on heat-
272 wave frequency, two important aspects need further elaboration. First note that the re-
273 lationship between the upper-tropospheric flow and surface temperature extremes is lin-
274 ear to such extent that a cyclonic monthly-mean anomaly reduces the likelihood of ex-
275 periencing a heatwave compared to typical flow conditions. Therefore, the geographi-
276 cally non-phase-locked stationary waves are less effective in causing a composite-mean
277 heatwave frequency signal than the troughs and ridges of the composite-mean wave train.
278 Secondly, a Rossby wave packet with a typical phase speed for boreal summer is slow
279 enough to facilitate a heatwave with minimum duration of 3 days. Therefore, the merid-
280 ional shift of Rossby wave packets is more relevant for summer heatwaves than the phase
281 speed change.

282 Another potential driver for mid-latitude continental heatwaves is interannual sea
283 surface temperature variability in the form of tropical-extratropical teleconnections (e.g.,
284 Luo & Lau, 2020; Wulff et al., 2017). In particular, the negative heatwave frequency anom-

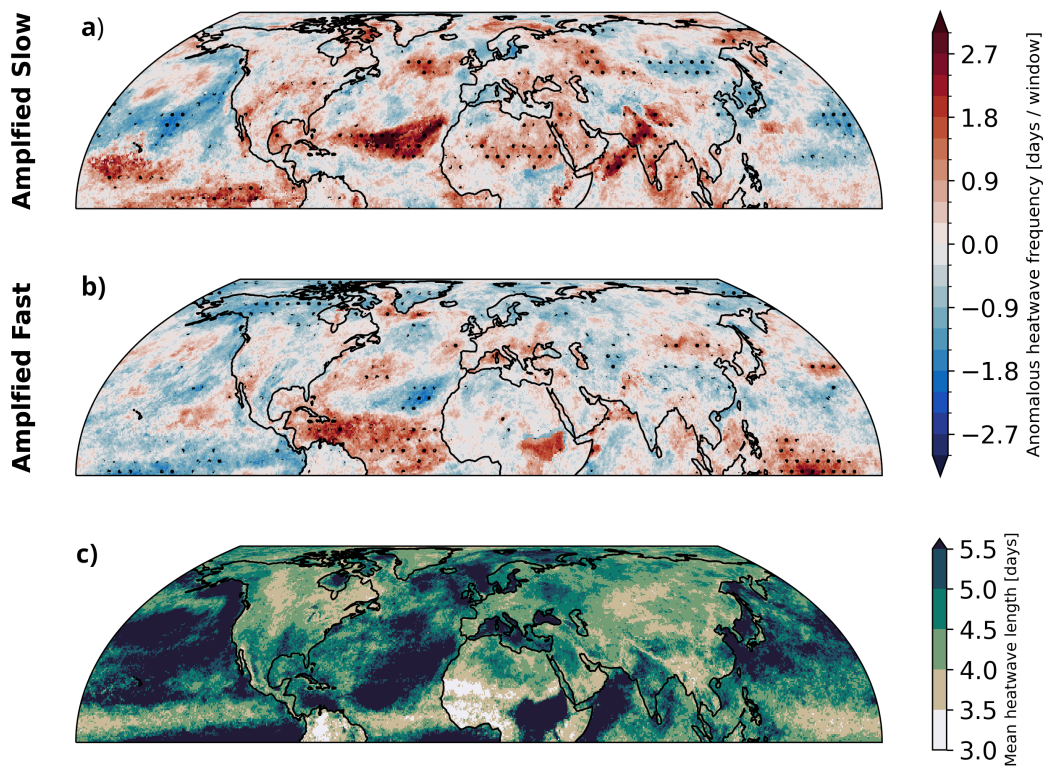


Figure 4. Mean heatwave frequency anomaly (panel a, b) for composites as defined for Figure 1 and the climatological boreal summer-mean heatwave duration (panel c). Stippling indicates a composite mean significantly different from zero at the 95% confidence level.

lies over the eastern tropical Pacific and positive anomalies over the western tropical Pacific for the "amplified fast" composite are reminiscent of sea surface temperature anomalies during the positive phase of El Niño-Southern Oscillation. This notion ties in well with the meridional shift in Rossby wave packet envelope in Figure 3 since there is a known relationship between El Niño and the extratropical storm track latitude: an equatorward storm track shift during the warm phase of El Niño has been reported over the Pacific, North America, and Europe (Fraedrich & Müller, 1992; Eichler & Higgins, 2006; Plante et al., 2015). On a similar note, the heatwave frequency anomalies over the North Atlantic for the "amplified fast" composite with a positive anomaly to the east of the United States flanked by negative anomalies to the north and south resemble the sea surface temperature tripole pattern associated with the positive phase of decadal North Atlantic Oscillation variability (e.g., Rodwell et al., 1999; Eden & Jung, 2001), another prominent mode of storm track variability.

4 Conclusions

Mid-latitude summer heatwaves are characterized as warm surface temperature extremes of a minimum duration of several days. When studying dynamical drivers, it is often assumed that persistent surface extremes require an anomalously persistent large-scale circulation in the form of amplified stationary waves (Petoukhov et al., 2013; Mann et al., 2017; Kornhuber et al., 2019; Di Capua et al., 2021). In this study, we evaluate this assumption using a categorical phase speed estimate based on spectral analysis of upper-tropospheric meridional wind. Cyclonic and anticyclonic circulation anomalies associated with the troughs and ridges of a geographically phase-locked stationary wave train cause a zonally asymmetric heatwave frequency response to changes in the phase speed of upper-tropospheric synoptic-scale waves. By shaping phase-locked stationary wave trains, phase speed is proven important for where, not whether summer heatwaves occur. An anomalously high upper-tropospheric flow persistence is, hence, not necessary for persistent warm extremes, in agreement with another recent study (Holmberg et al., 2022).

For understanding this conclusion, we highlight here that Rossby wave phase speed is a function of multiple variables. This study was designed to reduce the impact of certain covariates, for example by using a wavenumber dependant boundary between the "slow" and "fast" phase speed bin, but other covariates leave their trace in the composite-

317 analysis. In particular, we find an equatorward shift of Rossby wave packet envelopes
 318 during episodes of slow compared to fast phase propagation. The connection between
 319 the storm track latitude and the phase speed of mid-latitude waves has previously been
 320 noted and is potentially relevant for the circulation response to climate change (Chen
 321 & Held, 2007; Shaw et al., 2016). Other covariates for phase speed variability are sea sur-
 322 face temperature anomalies associated with El Niño or the North Atlantic Oscillation
 323 sea surface temperature tripole.

324 Our phase speed estimate tailored to measure hemispheric flow persistence is well
 325 reflected in the phase speed of localized Rossby wave packets. The consequential change
 326 in mean heatwave duration compared to the global average is, however, too weak to sig-
 327 nificantly alter heatwave frequency. This raises the question about limiting factors of heat-
 328 wave duration when the ridge of a wave packet is indeed stationary. Thermodynamic ef-
 329 fects, as for example latent heat release in ascending air masses upstream of the anti-
 330 cyclone (Black et al., 2004; Pfahl et al., 2015; Neal et al., 2022; White et al., 2023), most
 331 likely play a role.

332 Open Research Section

333 The ERA5 reanalysis data used in this study can be downloaded from the Coper-
 334 nicus ClimateData Store <https://doi.org/10.24381/cds.bd0915c6>. A repository with
 335 the python code for the data analysis is available from [https://doi.org/10.5281/zenodo](https://doi.org/10.5281/zenodo.10453988)
 336 .10453988.

337 Acknowledgments

338 The authors would like to thank Volkmar Wirth, Emmanuele Russo, and Andries
 339 de Vries for many fruitful discussions. This project has received funding from the Eu-
 340 ropean Research Council (ERC) under the European Union’s Horizon 2020 research and
 341 innovation programme (grant agreement No. 847456). Support from the Swiss National
 342 Science Foundation through project PP00P2_198896 to M.P. and D.D. is gratefully ac-
 343 knowledged. M.P. acknowledges financial support from the Collaborative Research on
 344 Science and Society (CROSS) Program of EPFL and UNIL.

345 **References**

- 346 Ali, S. M., Martius, O., & Röhlisberger, M. (2021). Recurrent rossby wave pack-
 347 ets modulate the persistence of dry and wet spells across the globe. *Geophysical Research Letters*, 48(5), e2020GL091452.
- 349 Black, E., Blackburn, M., Harrison, G., Hoskins, B., Methven, J., et al. (2004). Fac-
 350 tors contributing to the summer 2003 european heatwave. *Weather*, 59(8),
 351 217–223.
- 352 Chen, G., & Held, I. M. (2007). Phase speed spectra and the recent poleward
 353 shift of southern hemisphere surface westerlies. *Geophysical Research Letters*,
 354 34(21).
- 355 Coumou, D., Robinson, A., & Rahmstorf, S. (2013). Global increase in record-
 356 breaking monthly-mean temperatures. *Climatic Change*, 118(3), 771–782.
- 357 Di Capua, G., Sparrow, S., Kornhuber, K., Rousi, E., Osprey, S., Wallom, D., ...
 358 Coumou, D. (2021). Drivers behind the summer 2010 wave train leading to
 359 russian heatwave and pakistan flooding. *npj Climate and Atmospheric Science*,
 360 4(1), 55.
- 361 Domeisen, D. I., Eltahir, E. A., Fischer, E. M., Knutti, R., Perkins-Kirkpatrick,
 362 S. E., Schär, C., ... Wernli, H. (2023). Prediction and projection of heatwaves.
 363 *Nature Reviews Earth & Environment*, 4, 36–50. doi: <https://doi.org/10.1038/s43017-022-00371-z>
- 365 Ebi, K. L., Capon, A., Berry, P., Broderick, C., de Dear, R., Harenith, G., ... others
 366 (2021). Hot weather and heat extremes: health risks. *The lancet*, 398(10301),
 367 698–708.
- 368 Eden, C., & Jung, T. (2001). North atlantic interdecadal variability: oceanic re-
 369 sponse to the north atlantic oscillation (1865–1997). *Journal of Climate*, 14(5),
 370 676–691.
- 371 Eichler, T., & Higgins, W. (2006). Climatology and enso-related variability of
 372 north american extratropical cyclone activity. *Journal of Climate*, 19(10),
 373 2076–2093.
- 374 Fischer, E. M., & Knutti, R. (2015). Anthropogenic contribution to global occur-
 375 rence of heavy-precipitation and high-temperature extremes. *Nature climate
 376 change*, 5(6), 560–564.
- 377 Fischer, E. M., Seneviratne, S. I., Vidale, P. L., Lüthi, D., & Schär, C. (2007).

- 378 Soil moisture–atmosphere interactions during the 2003 european summer heat
379 wave. *Journal of Climate*, 20(20), 5081–5099.
- 380 Fraedrich, K., & Müller, K. (1992). Climate anomalies in europe associated with
381 enso extremes. *International Journal of Climatology*, 12(1), 25–31.
- 382 Fragkoulidis, G., & Wirth, V. (2020). Local rossby wave packet amplitude, phase
383 speed, and group velocity: Seasonal variability and their role in temperature
384 extremes. *Journal of Climate*, 33(20), 8767–8787.
- 385 Fragkoulidis, G., Wirth, V., Bossmann, P., & Fink, A. (2018). Linking northern
386 hemisphere temperature extremes to rossby wave packets. *Quarterly Journal of*
387 *the Royal Meteorological Society*, 144(711), 553–566.
- 388 García-Herrera, R., Díaz, J., Trigo, R. M., Luterbacher, J., & Fischer, E. M. (2010).
389 A review of the european summer heat wave of 2003. *Critical Reviews in Envi-*
390 *ronmental Science and Technology*, 40(4), 267–306.
- 391 Hauser, M., Orth, R., & Seneviratne, S. I. (2016). Role of soil moisture versus recent
392 climate change for the 2010 heat wave in western russia. *Geophysical Research*
393 *Letters*, 43(6), 2819–2826.
- 394 Hayashi, Y. (1979). A generalized method of resolving transient disturbances into
395 standing and traveling waves by space-time spectral analysis. *Journal of Atmo-*
396 *spheric Sciences*, 36(6), 1017–1029.
- 397 Hersbach, H., Bell, B., Berrisford, P., Hirahara, S., Horányi, A., Muñoz-Sabater, J.,
398 ... others (2020). The era5 global reanalysis. *Quarterly Journal of the Royal*
399 *Meteorological Society*, 146(730), 1999–2049.
- 400 Holmberg, E., Messori, G., Caballero, R., & Faranda, D. (2022). The counter-
401 intuitive link between european heatwaves and atmospheric persistence. *Earth*
402 *System Dynamics Discussions*, 1–26.
- 403 Jiménez-Esteve, B., & Domeisen, D. I. (2022). The role of atmospheric dynam-
404 ics and large-scale topography in driving heatwaves. *Quarterly Journal of the*
405 *Royal Meteorological Society*, 148(746), 2344–2367.
- 406 Jiménez-Esteve, B., Kornhuber, K., & Domeisen, D. (2022). Heat extremes driven
407 by amplification of phase-locked circumglobal waves forced by topography
408 in an idealized atmospheric model. *Geophysical Research Letters*, 49(21),
409 e2021GL096337.
- 410 Kornhuber, K., Osprey, S., Coumou, D., Petri, S., Petoukhov, V., Rahmstorf, S., &

- 411 Gray, L. (2019). Extreme weather events in early summer 2018 connected by a
412 recurrent hemispheric wave-7 pattern. *Environmental Research Letters*, 14(5),
413 054002.
- 414 Luo, M., & Lau, N.-C. (2020). Summer heat extremes in northern continents linked
415 to developing enso events. *Environmental Research Letters*, 15(7), 074042.
- 416 Mann, M. E., Rahmstorf, S., Kornhuber, K., Steinman, B. A., Miller, S. K., &
417 Coumou, D. (2017). Influence of anthropogenic climate change on planetary
418 wave resonance and extreme weather events. *Scientific reports*, 7(1), 1–12.
- 419 Meehl, G. A., & Tebaldi, C. (2004). More intense, more frequent, and longer lasting
420 heat waves in the 21st century. *Science*, 305(5686), 994–997.
- 421 Miralles, D. G., Teuling, A. J., Van Heerwaarden, C. C., & Vilà-Guerau de Arellano,
422 J. (2014). Mega-heatwave temperatures due to combined soil desiccation and
423 atmospheric heat accumulation. *Nature geoscience*, 7(5), 345–349.
- 424 Neal, E., Huang, C. S., & Nakamura, N. (2022). The 2021 pacific northwest heat
425 wave and associated blocking: meteorology and the role of an upstream cy-
426 clone as a diabatic source of wave activity. *Geophysical Research Letters*,
427 49(8), e2021GL097699.
- 428 Petoukhov, V., Rahmstorf, S., Petri, S., & Schellnhuber, H. J. (2013). Quasiresonant
429 amplification of planetary waves and recent northern hemisphere weather ex-
430 tremes. *Proceedings of the National Academy of Sciences*, 110(14), 5336–5341.
- 431 Pfahl, S., Schwierz, C., Croci-Maspoli, M., Grams, C. M., & Wernli, H. (2015).
432 Importance of latent heat release in ascending air streams for atmospheric
433 blocking. *Nature Geoscience*, 8(8), 610–614.
- 434 Pfahl, S., & Wernli, H. (2012). Quantifying the relevance of atmospheric blocking for
435 co-located temperature extremes in the northern hemisphere on (sub-) daily
436 time scales. *Geophysical Research Letters*, 39(12).
- 437 Plante, M., Son, S.-W., Atallah, E., Gyakum, J., & Grise, K. (2015). Extratropical
438 cyclone climatology across eastern canada. *International Journal of Climatol-
439 ogy*, 35(10), 2759–2776.
- 440 Randel, W. J., & Held, I. M. (1991). Phase speed spectra of transient eddy fluxes
441 and critical layer absorption. *Journal of the atmospheric sciences*, 48(5), 688–
442 697.
- 443 Riboldi, J., Lott, F., d'Andrea, F., & Rivière, G. (2020). On the linkage between

- 444 rossby wave phase speed, atmospheric blocking, and arctic amplification. *Geo-*
445 *physical Research Letters*, 47(19), e2020GL087796.
- 446 Rodwell, M. J., Rowell, D. P., & Folland, C. K. (1999). Oceanic forcing of the win-
447 tertime north atlantic oscillation and european climate. *Nature*, 398(6725),
448 320–323.
- 449 Rossby, C.-G. (1945). On the propagation of frequencies and energy in certain types
450 of oceanic and atmospheric waves. *Journal of the Atmospheric Sciences*, 2(4),
451 187–204.
- 452 Röthlisberger, M., Frossard, L., Bosart, L. F., Keyser, D., & Martius, O. (2019). Re-
453 current synoptic-scale rossby wave patterns and their effect on the persistence
454 of cold and hot spells. *Journal of Climate*, 32(11), 3207–3226.
- 455 Röthlisberger, M., Pfahl, S., & Martius, O. (2016). Regional-scale jet waviness mod-
456 ulates the occurrence of midlatitude weather extremes. *Geophysical Research
457 Letters*, 43(20), 10–989.
- 458 Russo, E., & Domeisen, D. I. (2023). Increasing intensity of extreme heatwaves: the
459 crucial role of metrics. *Geophysical Research Letters*, 50(14), e2023GL103540.
- 460 Russo, S., Sillmann, J., & Fischer, E. M. (2015). Top ten european heatwaves since
461 1950 and their occurrence in the coming decades. *Environmental Research Let-
462 ters*, 10(12), 124003.
- 463 Schneidereit, A., Schubert, S., Vargin, P., Lunkeit, F., Zhu, X., Peters, D. H., &
464 Fraedrich, K. (2012). Large-scale flow and the long-lasting blocking high over
465 russia: Summer 2010. *Monthly Weather Review*, 140(9), 2967–2981.
- 466 Shaw, T., Baldwin, M., Barnes, E. A., Caballero, R., Garfinkel, C., Hwang, Y.-T.,
467 ... others (2016). Storm track processes and the opposing influences of climate
468 change. *Nature Geoscience*, 9(9), 656–664.
- 469 Simmons, A. J., & Hoskins, B. J. (1979). The downstream and upstream develop-
470 ment of unstable baroclinic waves. *Journal of the Atmospheric Sciences*, 36(7),
471 1239–1254.
- 472 Sousa, P. M., Trigo, R. M., Barriopedro, D., Soares, P. M., & Santos, J. A. (2018).
473 European temperature responses to blocking and ridge regional patterns. *Cli-
474 mate Dynamics*, 50, 457–477.
- 475 White, R. H., Anderson, S., Booth, J. F., Braich, G., Draeger, C., Fei, C., ... others
476 (2023). The unprecedeted pacific northwest heatwave of june 2021. *Nature*

- 477 *Communications*, 14(1), 727.
- 478 White, R. H., Kornhuber, K., Martius, O., & Wirth, V. (2022). From atmospheric
479 waves to heatwaves: A waveguide perspective for understanding and predict-
480 ing concurrent, persistent, and extreme extratropical weather. *Bulletin of the*
481 *American Meteorological Society*, 103(3), E923–E935.
- 482 Wirth, V. (2020). Waveguidability of idealized midlatitude jets and the limitations
483 of ray tracing theory. *Weather and Climate Dynamics*, 1(1), 111–125.
- 484 Wirth, V., & Polster, C. (2021). The problem of diagnosing jet waveguidability in
485 the presence of large-amplitude eddies. *Journal of the Atmospheric Sciences*,
486 78(10), 3137–3151.
- 487 Wirth, V., Riemer, M., Chang, E. K., & Martius, O. (2018). Rossby wave packets on
488 the midlatitude waveguide—a review. *Monthly Weather Review*, 146(7), 1965–
489 2001.
- 490 Wulff, C. O., Greatbatch, R. J., Domeisen, D. I., Gollan, G., & Hansen, F. (2017).
491 Tropical forcing of the summer east atlantic pattern. *Geophysical Research Let-*
492 *ters*, 44(21), 11–166.
- 493 Yeh, T.-c. (1949). On energy dispersion in the atmosphere. *Journal of Atmospheric*
494 *Sciences*, 6(1), 1–16.
- 495 Yiou, P., Cattiaux, J., Faranda, D., Kadygrov, N., Jézéquel, A., Naveau, P., ... oth-
496 ers (2020). Analyses of the northern european summer heatwave of 2018.
497 *Bulletin of the American Meteorological Society*, 101(1), S35–S40.
- 498 Zimin, A. V., Szunyogh, I., Patil, D., Hunt, B. R., & Ott, E. (2003). Extracting en-
499 velopes of rossby wave packets. *Monthly weather review*, 131(5), 1011–1017.
- 500 Zschenderlein, P., Fragkoulidis, G., Fink, A. H., & Wirth, V. (2018). Large-scale
501 rossby wave and synoptic-scale dynamic analyses of the unusually late 2016
502 heatwave over europe. *Weather*, 73(9), 275–283.